Journal of Energy Storage 35 (2021) 102304

Contents lists available at ScienceDirect

Journal of Energy Storage

journal homepage: www.elsevier.com/locate/est

Comparison of methods for finding the capacitance of a supercapacitor

L.E. Helseth

Department of Physics and Technology, Allegaten 55, 5020 Bergen, University of Bergen, Norway

ARTICLE INFO

Keywords:
Supercapacitor
Energy storage
Capacitance

ABSTRACT

A carbon-based supercapacitor is usually associated with a capacitance such that the user can access its ability to store electrical charge. Three different measurement methods or variations thereof are typically employed to find the capacitance; galvanostatic charging, cyclic voltammetry and impedance spectroscopy. These three methods may give rather different capacitances, which must be interpreted with care. Here, it is discussed how one can extract consistent capacitance values from measurements obtained with the three techniques, to be interpreted within a single dynamic equivalent circuit. Different methods are compared in order to demonstrate where systematic errors occur, and how and under which conditions they can be removed. The extension of the methods presented here to pseudocapacitors utilizing both Faradaic and non-Faradaic charge storage is also briefly discussed.

1. Introduction

Supercapacitors, often also called electrochemical double layer capacitors, are based on porous carbon structures immersed in an electrolyte [1–4]. The electrical double layer formed by ions at the porous carbon surface is responsible for the large amount of charge that a supercapacitor can store [5–8]. The behavior of supercapacitors has been modelled using microscopic models [9–12] as well as different electrical equivalent circuits [13–39]. These equivalent circuit models have found widespread use also in practical applications, whenever quick and computationally efficient analysis is required.

A crucial parameter of a supercapacitor is its capacitance. Three different measurement methods, or variants thereof, are often employed to find the capacitance; galvanostatic charging, cyclic voltammetry and impedance spectroscopy. In the electrochemical literature on electrical double layers one distinguishes between integral and differential capacitance [40]. This distinction has sometimes also been used when analyzing supercapacitors [41–45]. While the integral capacitance is often extracted from galvanostatic charging and cyclic voltammetry experiments, differential capacitance can be obtained from impedance spectroscopy measurements. Care is often taken to distinguish the two definitions [42,45] or to make analysis methods or electrical measurement setups to improve the correctness of the measured capacitance values [4,44]. While there are inherent differences in the methods used for extracting capacitance values from galvanostatic charging, cyclic voltammetry and impedance spectroscopy, it would be beneficial to be able to extract capacitance values that are consistent within the experimental errors and that can be interpreted within a single equivalent circuit. In the current study supercapacitors utilizing non-Faradaic charge storage in the electrical double layer are addressed, and the capacitances obtained using the three different methods are compared in order to demonstrate where systematic errors occur, and how and under which conditions the errors can be removed. At the end it is also briefly discussed how the methods can be extended to pseudocapacitors where both Faradaic and non-Faradaic charge storage play roles.

2. The dynamic equivalent circuit and the two definitions of capacitance

Consider the supercapacitor structure as visualized in Fig. 1.

We note first that there is a resistance contribution R_{s1} due to contact with the metal electrode and R_{si} due to the separator, and so on. These latter contributions sum up to a single resistance which hereafter will be denoted R_s. One can then imagine that for each carbon grain, there is an electrical double layer that allows a displacement current $I_{di}=A_i\varepsilon_0\varepsilon_r\partial E_i/\partial t$, where A_i is the local area, ε_r is the relative permittivity, ε_0 the permittivity of vacuum and E_i the local electrical field. In addition, there is also a resistive current I_{ri} which could be due to local resistive paths between grains in the electrolyte as well as flaws in the electrical double layer. In the simplest approximation, also called Ohms law, there is a linear relationship between the resistive current and the applied electric field according to $I_{ri}=A_i\sigma_i E_i$, where σ_i is the local conductivity. The sum of the displacement and resistive current elemental contributions give $I=I_{di}+I_{ri}=A_i\varepsilon_0\varepsilon_r\partial E_i/\partial t+A_i\sigma_i E_i$. We here assume that this current follows a path through the porous carbon + electrolyte system, thus forming an equivalent circuit as seen in Fig. 1. If one now assumes that the local grain voltage U_i over the double layer is proportional to the electric field such that $E_i=U_i/d_i$, where d_i has unit thickness but is here

https://doi.org/10.1016/j.est.2021.102304
Received 2 November 2020; Received in revised form 17 December 2020; Accepted 12 January 2021
Available online 21 January 2021

treated merely as a proportionality constant, one may write the current as

$$I = \frac{U_i}{R_i} + C_i \frac{dU_i}{dt}, \tag{1}$$

where $R_i=d_i/(\sigma_i A_i)$ is a measure of the local resistance and $C_i=\varepsilon_0\varepsilon_r A_i/d_i$ is a measure of the local capacitance. It should be emphasized Eq. (1) is not based on a formal derivation, but rather a semi-empirical justification leading to the equivalent circuit in fig.1 using linearized equations. For example, the given capacitance would only be reasonable for a flat electrical double layer under the condition of small voltages [40]. That is, the C_i does not explicitly account for the known voltage-dependence of supercapacitors, although this problem could perhaps be fixed empirically if one allowed the voltage-dependence to be lumped into the parameter d_i. In most situations one treats the constants R_i and C_i as fitting constants, and the type of equivalent circuit seen in fig.1 resulting from the semi-empirical arguments above has been used extensively to model supercapacitors [24, 26, 27, 37], and can also be justified by linearization of the microscopic equations governing drift and diffusion. For these reasons, the equivalent circuit of Fig. 1 is selected as the starting point of finding the capacitance of a supercapacitor in the current study. A key observation is that Eq. (1) is a sum of two terms, one dissipative and one capacitive. The capacitance should only be related to the latter one, and one should be careful not to mix these two contributions when extracting this property.

It must be mentioned that nonlinear contributions might occur for higher fields. It is also clear that additional contribution occurs if redox-reactions are present such as in pseudocapacitors. Recent works have put emphasis on the distinction between capacitive and battery-like behavior from the current-voltage diagrams [46,47], and the near linearity between current and applied electric field or voltage has been used as an indicator of capacitive or pseudocapacitive behavior [46]. However, there is still a need to know how to extract capacitance for such energy storage systems. In ref. [48] a careful comparison between two methods yielded considerable differences, which could be interpreted using a five-branch ladder equivalent circuit. In the current work, a different approach is proposed utilizing the equivalent circuit of Fig. 1, where the resistive contributions are explicitly removed before extracting the capacitance.

To see how the standard definitions of capacitance may lead to trouble, a situation with only one ($i=1$) of the elemental circuits in Fig. 1 is considered. Setting $U_1(t=0)=0$ and $U_1(t)=U$, gives the following total charge accumulated and passed through the supercapacitor upon integrating Eq. (1),

$$q = \frac{1}{R_1}\int_0^t U(t)dt + C_1 U. \tag{2}$$

One can now define the integral capacitance as

$$C_{int} = \frac{q}{U} = \frac{1}{R_1}\frac{\int_0^t U(t)dt}{U} + C_1, \tag{3}$$

and the differential capacitance as

$$C_{diff} = \frac{dq}{dU} = \frac{1}{R_1}\frac{U}{\frac{dU}{dt}} + C_1. \tag{4}$$

From Eqs. (3) and (4) it is seen that unless $R\to\infty$, one obtains $C_{diff}\neq C_{int}$. Thus, the definitions of integral and differential capacitances cannot be directly used to extract values of the capacitance that can be compared with what we normally associate with the term, since they both mix together resistive and displacement contributions. One could argue that one should subtract the second term in Eqs. (3) and (4) to get rid of the resistive contribution. That is, in the case of Eq. (4) one could use $C_1=C_{diff} - U/(R_1 dU/dt)$ instead of C_{diff} as a measure of the capacitance. Similarly, for Eq. (3). One problem with this approach is that while U and dU/dt are directly measurable quantities, R_1 must be deduced from the experiments based on some model. Another issue is that each measurement technique relies on unique measurement procedures that might not be optimally suited to this definition. In the following, it will be shown alternative and perhaps more direct manners to extract capacitance directly using the equivalent circuit in Fig. 1 in the case of galvanostatic charging, cyclic voltammetry and impedance spectroscopy. To this end, it should also be mentioned that at high frequencies sometimes encountered in impedance spectroscopy, one also has to account for a serial inductance L, not shown in Fig. 1.

3. Experimental details

The goal of this work is to detail the methods for extracting capacitance, not to do extensive testing of a range of devices. Therefore, a GoldCap supercapacitor of nominal capacitance 10 F and voltage 2.5 V was used to demonstrate the methods proposed. Current and voltage measurements were done with either a Biologic SP050 or a Gamry Ref. 600. During galvanostatic charging currents ranging from 0.1 A to 0.8 A were imposed, while the current fluctuations remained below ±0.1 mA and the voltage fluctuations about ±0.1 mV. Cyclic voltammetry was undertaken at 50 mV/s. Galvanostatic impedance

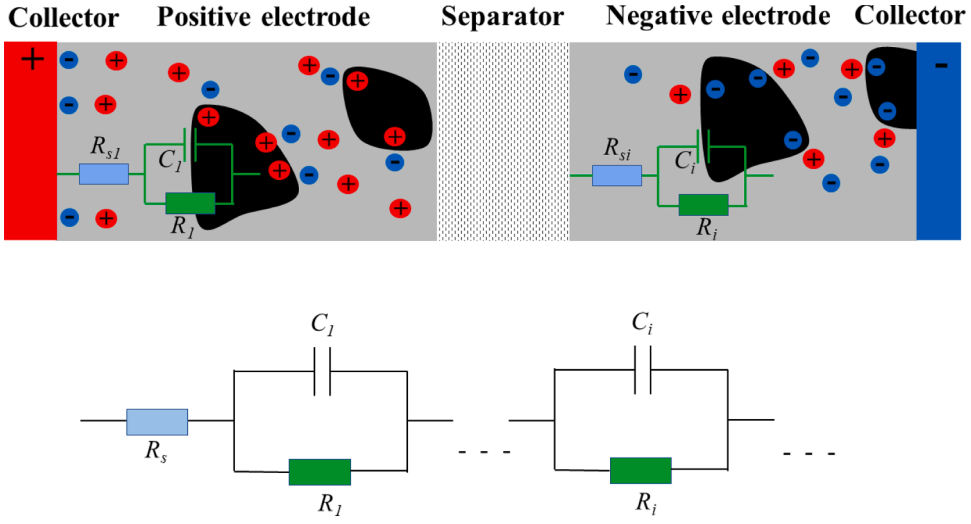

Fig. 1. Schematic drawing of the interior of a supercapacitor (top) and the corresponding equivalent circuit used in this study (bottom).

spectroscopy done in the frequency range 2 mHz to 1 MHz with 50 mA root-mean-square about zero average current.

4. Galvanostatic charging

The capacitance is often extracted during galvanostatic charging where the current I_0=dq/dt is held constant while the voltage is measured. If one neglects non-capacitive behavior and assumes that the charge at any point in time is given by $q=C_{int}V_c$, where C_{int} is the integral capacitance and V_c is the symbol for the voltage over the capacitor to distinguish from the voltage U used in Eqs. (3) and (4). It follows that both the integral and differential capacitance can be given by $C_{int}=C_{diff}=I_0/(\mathrm{d}V_c/\mathrm{d}t)$ for any measured voltage rate $dV_c/dt>0$. A significant problem with this approach is that it assumes that all the charge is associated with the capacitive element, thus neglecting any resistive losses. To find the capacitance, one needs to consider the resistive elements as well.

Fig. 2 a) shows the measured voltage V_c over the supercapacitor used in this study as it is exposed to a constant current $I_0=0.1$ A (red line), $I_0=0.3$ A (green line) and $I_0=0.7$ A (blue line) starting at $t=0$ s. In the inset of Fig. 2 a) it is seen that there is an initial jump V_b in the voltage when current is applied, and this is associated with a series resistor R_s as has been detailed in previous works [13, 33, 49]. In Fig. 2 c) it is seen that the voltage jump V_b is directly proportional to the applied current I_0, thus suggesting a relationship $V_b=R_sI_0$ for this particular supercapacitor, with $R_s=(37\pm1)$ mΩ.

Except for the initial jump V_b, the voltage V_c versus time curves in Fig. 2 a) appear to have a constant slope if one observes it only over a limited initial time interval, which means that at small times it might be useful to model the supercapacitor as an ideal capacitor in series with a resistor R_s. However, if one monitors the voltage over the supercapacitor over a longer period of time, as in Fig. 2 a), it is observed that the curve is no longer linear in time, but instead exhibit a nonlinear behavior indicating deviation from the simple model of an ideal capacitor in series with a resistor. An estimate of the capacitance based on the formula $C_{int}=C_{diff}=I_0/(\mathrm{d}V_c/\mathrm{d}t)$ may then lead to systematic errors if sufficient care is not taken. That is, it is seen from Fig. 2 c) that the rate dV_c/dt decreases with time, and one needs to know if any of the time intervals are more appropriate than others when estimating the capacitance.

One way to extract the capacitance is to consider the dynamic equivalent model shown in Fig. 1. First consider a capacitance C_j and a resistance R_j, in parallel. The supercapacitor can be represented by N such parallel-connected elements in series, and they are also series-connected to the resistance R_s. The charges Q_i on each of the capacitors are assumed to follow a linear charge-voltage relationship, and the voltage over the capacitors C_i and resistors R_i can be given by

$$\frac{Q_i}{C_i} = R_i I_{R_i}, \tag{5}$$

where I_{Ri} is the current through resistor R_i. The total constant current I_0 is then found to be the sum of the current through one capacitor C_i and one resistor R_i such that

$$I_0 = I_{C_i} + I_{R_i} = \frac{dQ_i}{dt} + \frac{Q_i}{R_iC_i}. \tag{6}$$

Solving this differential equation gives the charge on each capacitive element after a time t as

$$Q_i(t) = Q_i(0)e^{-\frac{t}{\tau_i}} + I_0\tau_i\left(1 - e^{-\frac{t}{\tau_i}}\right), \tau_i = R_iC_i \tag{7}$$

In the current study the galvanostatic charging starts when $Q_i(t=0)=0$, such that the voltage $V_c(t) = \sum_{i=1}^{N}\frac{Q_i}{C_i} + R_sI_0$ over the entire supercapacitor is given by

$$V_c(t) = I_0\sum_{i=1}^{N} R_i\left(1 - e^{-t/\tau_i}\right) + R_sI_0. \tag{8}$$

The rate of change can then be written as

$$\frac{dV_c(t)}{dt} = \sum_{i=1}^{N}\frac{I_0}{C_i}e^{-t/\tau_i}. \tag{9}$$

For small times, $t<<\tau_i$, the equivalent capacitance C_{eq} can be determined from the constant current and the voltage rate as

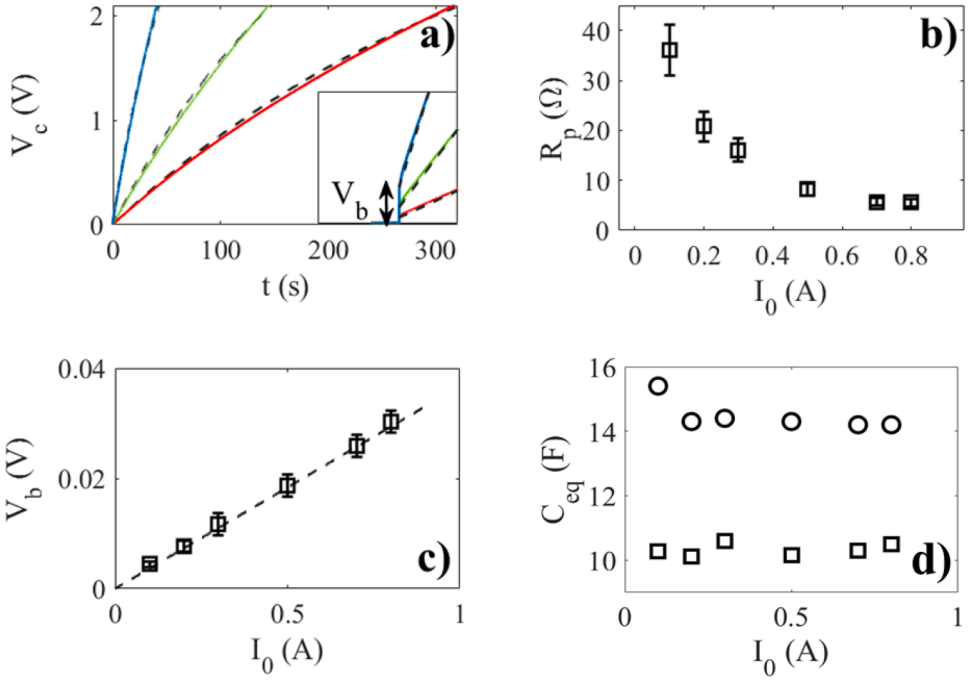

Fig. 2. In a) the voltage measured during galvanostatic charging is seen for $I_0=0.1$ A (red line), 0.3 A (green line) and 0.7 A (blue line). The black, dashed lines are corresponding fits using Eq. (11). The inset in a) shows the short-time dynamics the first 2.5 seconds along with the initial voltage jump V_b. In b) the parallel resistance R_1 is shown as function of current. In c) the squares show the voltage jump V_b is shown as function of current, and the dashed line is a linear fit $V_b=R_sI_0$ with $R_s=(37\pm1)$ mΩ. In d), the capacitance extracted using Eq. (10) (squares) and the capacitance extracted using the average slope $<dV_c/dt>$ (circles) is shown (For interpretation of the references to color in this figure legend, the reader is referred to the web version of this article.).

$$\frac{1}{\sum_{i=1}^{N}\frac{1}{C_i}} = C_{eq} \approx \frac{I_0}{\left(\frac{dV_c(t)}{dt}\right)_{t\ll\tau_i}}. \tag{10}$$

From Eq. (10) it is seen that the equivalent capacitance C_{eq} due to series-connected capacitors C_i is what we find when evaluating the ratio of the current and the initial slope $(dV_c/dt)_{t<<\tau i}$. By computing the average voltage rate over the first second after applying a current, the equivalent capacitance was found to be C_{eq}=*10.28, 10.11, 10.59, 10.15, 10.29* and *10.50 F* for I_0=*0.1 A, 0.2 A, 0.3 A, 0.5 A, 0.7 A* and *0.8 A*. Thus, for the six different currents the average capacitance was *10.3 F* with a standard deviation *0.2 F*, thus demonstrating that C_{eq} remains constant as the current changes. It should be clear that this approach does not allow one to estimate the individual capacitances C_i. Moreover, one must be considering the initial voltage rate $(dV_c/dt)_{t<<\tau i}$ only. One can compare these values with those obtained using the standard approach for extracting the capacitance based on the formula $C_{eq}=I_0/(<dV_c/dt>)$, where $<dV_c/dt>$ is the average slope over the entire measured time interval. The values obtained using this formula are shown in Fig. 2 d) as circles, along with the capacitance values extracted from Eq. (10) as squares. It is noted that the standard approach results in erroneously low slopes since resistive contributions are neglected, and therefore about 4 F higher capacitances than the approach using Eq. (10). When comparing the data with other techniques in the subsequent sections, it will further be shown that the approach based on Eq. (10) is superior to the standard technique, thus avoiding unnecessary systematic errors.

In order to understand the long-term behavior of the voltage V_c during galvanostatic charging, one needs to know the number of circuits *N* in Eq. (8). However, without additional information, it is impossible to extract this information from the voltage data alone. One could make a sequential fit with gradually increasing N until one gets the accuracy one is looking for. That is, one starts with *N=1* and observe how well it fits the experimental data. In that case, Eq. (8) reduces to

$$V_c(t) = I_0R_1\left(1-e^{-t/\tau_1}\right) + R_sI_0. \tag{11}$$

where $\tau_1=R_1C_1$ and it will be assumed that the obtained values for C_{eq} above can be used to determine C_1. R_s is already determined from Fig. 2 c). By fitting Eq. (11) to the curves like those of Fig. 2 a) with $R^2>0.99$, the values for R_1 were obtained as shown in Fig. 2 b). If one wishes to obtain an even better fit, one has to use the fitted values for R_1, C_1 and R_s obtained with *N=1*, and insert into Eq. (8) with *N=2* to obtain two new fitting constants R_2 and C_2. Furthermore, if the obtained fit is still not good enough, one has to continue this procedure until one obtains the value of R^2 one is looking for. In the example of Fig. 2 a) a fit with $R^2>0.99$ is deemed good enough for a proper comparison of capacitance values between techniques, thus allowing use of only one fitting round with *N=1*.

From Fig. 2 a) it can be seen that the voltage V_c initially follows a linear curve represented by Eq. (11) for $t<<\tau_1$ as $V_c\approx I_0t/C_1$. For larger values of *t*, it is found that dV_c/dt decreases with time due to the fact that R_1 starts to play a role, such that V_c deviates from its initial linear behavior. The larger the charging current, the faster the decrease in the slope dV_c/dt.

The approach proposed here to analyze galvanostatic charging allows one to extract a current-independent capacitance $C_{eq}\approx C_1$, while the parallel resistance R_1 decreases with increasing current before it reaches a limiting value of about *5 Ω* as the current approaches *1 A*. This can be interpreted as the time constant for charge transfer into and out of the pores in the supercapacitor decreases the stronger the applied current is. We note that the approach used here for galvanostatic charging is similar to the traditional approach in most respects, except one. For Eq. (10) to be valid, only small times ($t<<\tau_i$) should be considered. If one wants to apply the equation for larger times one needs to include a correction factor according to Eq. (9).

5. Cyclic voltammetry

Cyclic voltammetry is another popular method for determining the capacitance of a supercapacitor. It is often used to study single electrodes using three-electrode arrangement, but also fully assembled two-electrode supercapacitors have been studied [44]. When determining capacitance using cyclic voltammetry, one applies a sawtooth voltage across the capacitor and simultaneously measure the resulting current.

A typical cyclic voltammogram of the nominal *10 F* supercapacitor is shown in Fig. 3 a) for a rate dV_c/dt=*50 mV/s*. The current is measured while the voltage reaches a maximum value of *0.1 V* (red curve), *0.3 V* (orange curve), *0.5 V* (brown curve), *0.7 V* (black curve), *1.0 V* (green curve), *1.3 V* (blue curve) and *1.5 V* (violet curve).

The most common approach to find the capacitance using cyclic voltammetry is to assume that the entire charge *q* is deposited on the capacitive element, such that the charge, the integral capacitance and the voltage measured are related as $q=C_{int}V_c$. Assuming a constant integral capacitance during charging by a constant rate dV_c/dt, the current can be written as $I=C_{int}dV_c/dt$. The integral capacitance is therefore given by $C_{int}=I/(dV_c/dt)$, which is a formula often used in the literature to determine capacitance in supercapacitors and pseudocapacitors [50–54]. A problem with this approach is that the current is hardly ever constant during a cyclic voltammogram. It has therefore been suggested to use low voltage rates or certain voltage regions to obtain more accurate values of the capacitance [16]. However, this is not always feasible, and one way that is sometimes used to account for this problem is to find the average current $<I>$ in a certain voltage range where it appears not to change too much, resulting in a capacitance given by

$$C_{eff} = \frac{\langle I\rangle}{\frac{dV_c}{dt}}. \tag{12}$$

Here, the denotation C_{eff} is used to distinguish the capacitance obtained from C_{eq} using galvanostatic charging. The green triangles in Fig. 3 b)

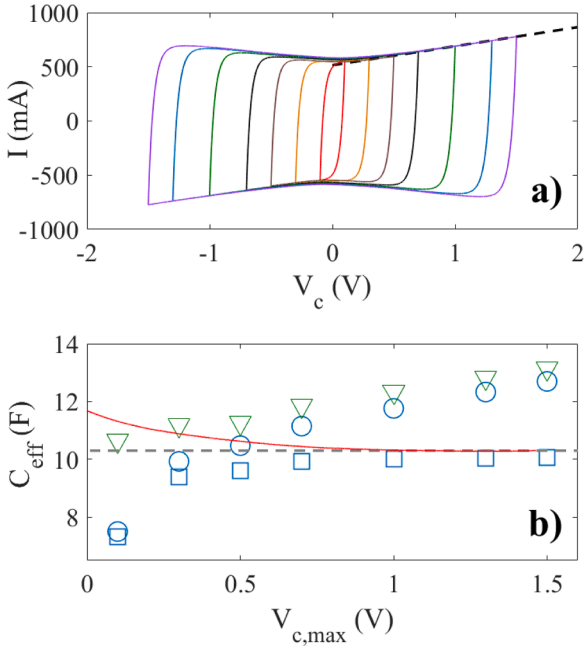

Fig. 3. In a), the cyclic voltammogram is shown as a function of current for a rate dV_c/dt=*50 mV/s* while the voltage reaches a maximum value of *0.1 V* (red curve), *0.3 V* (orange curve), *0.5 V* (brown curve), *0.7 V* (black curve), *1.0 V* (green curve), *1.3 V* (blue curve) and *1.5 V* (violet curve).
In b) the effective capacitance C_{eff} extracted using the methods described in the text. The dashed brown line is the capacitance of *10.3 F* extracted from galvanostatic charging(For interpretation of the references to color in this figure legend, the reader is referred to the web version of this article.).

show the extracted effective capacitance C_{eff} obtained from the cyclic voltammograms in Fig. 3 a). The capacitance was extracted by computing the average value of the current in the upper right quadrant between zero and maximum voltage. Since the current increases with applied voltage V_c, the average current and therefore also the effective capacitance increases as well. It is seen that the effective capacitance varies between about *10 F* and *14 F*, and that systematic deviations occur from the value of *(10.3±0.2) F* obtained using galvanostatic charging shown as a dashed brown line.

The large systematic errors in the obtained effective capacitance using the simple averaging method is mainly due to the fact that it neglects the resistive elements which cause an increase in the current with applied voltage. The question is whether one can find a simple method using cyclic voltammetry to determine the capacitance without introducing systematic errors. To this end, it is convenient to return to the dynamic equivalent circuit model of Fig. 1, where the voltage over the supercapacitor is given by

$$V_c = \sum_{i=1}^{N} \frac{Q_i}{C_i} + R_s I. \tag{13}$$

Assume now that one applies a constant rate dV_c/dt over the supercapacitor, where $\frac{dV_c}{dt} = \sum_{i=1}^{N} \frac{I_i}{C_i} + R_s \frac{dI}{dt}$. In general, one does not know the currents through the various branches, and then the full formula is required. However, as demonstrated in the previous section, $N=1$ is often a good approximation. It will also be assumed that the voltage over the parallel resistor R_1 is much larger than the series resistor, $R_1 I_{R_1} \gg I R_s$, which is reasonable when the series resistance is of the order of *0.04 Ω* as seen in the previous section. If these conditions are fulfilled, one can write

$$\frac{1}{R_s}\frac{dV_c}{dt} + \frac{V_c}{R_s R_1 C_1} = \frac{dI}{dt} + \frac{I}{R_s C_1}. \tag{14}$$

Assuming that the initial current is $I(t=0)=0$, this first-order differential equation has solution

$$I(t) = C_1 \frac{dV_c}{dt}\left(1 - e^{-t/\tau_s}\right) + \frac{1}{R_1}\frac{dV_c}{dt}\left[t - \tau_s\left(1 - e^{-t/\tau_s}\right)\right], \quad \tau_s = R_s C_1 \tag{15}$$

The solid line in Fig. 4 is a plot of the measured current over the supercapacitor as a function of time during a cyclic voltammogram, whereas the dashed line is a fit to Eq. (15) with $C_1=10.3$ *F* and $R_1=6.5$ *Ω* and $R_s=50$ *mΩ*. It should be noted that initially the term containing $C_1 dV_c/dt$ dominates. The voltage increases linearly with time according to $V_c=(dV_c/dt)t$, and eventually the second term containing $(1/R_1)dV_c/dt$ becomes important. When $t>>\tau_s \approx 0.4$*s*, the black dashed line in Fig. 3 a) suggests that the current increases with voltage as $I(t)=C_1 dV_c/dt+V_c(t)/R_1$.

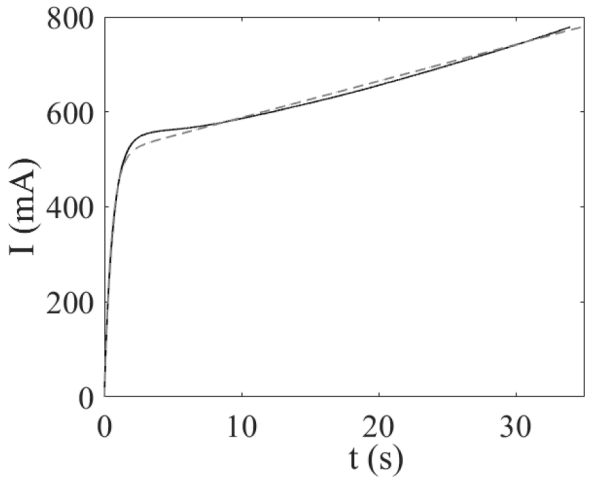

Fig. 4. The solid line is the measured current as a function of time during a cyclic voltammogram, whereas the dashed line is a fit to Eq. (15) with $C_1=10.3$ *F* and $R_1=6.5$ *Ω* and $R_s=50$ *mΩ*.

From the equation $I(t)=C_1 dV_c/dt+V_c(t)/R_1$, which is analogous to Eq. (1), the capacitance can be estimated as

$$C_{eff} = C_1 \approx \frac{I(t) - \frac{V_c(t)}{R_1}}{\frac{dV_c}{dt}}. \tag{16}$$

Here, the resistive contribution has been explicitly removed such that only the capacitive part remains. The effective capacitance in Eq. (16) can be computed for every current-voltage data point in the cyclic voltammogram, although one cannot use the data points near the turning points where the voltage rate dV_c/dt changes sign. Thus, a continuous curve of effective capacitances can be obtained. It is noted that these effective capacitances only converge to a given value when $t>>\tau_s$, for which $I(t)=C_1 dV_c/dt+V_c(t)/R_1$ is valid. As an example, the red solid line in Fig. 3 b) shows the effective capacitance computed from Eq. (16) using the upper right quadrant of the *1.5 V* curve (violet curve) in Fig. 3 a). The values obtained converge to *10.3 F* when $V_{c,max} > 1$ *V* ($t>>\tau_s$), which is consistent with the value *(10.3±0.2) F* found using galvanostatic charging.

In many situations it might be more convenient to deal with the area of the cyclic voltammogram directly, as reported in e.g. refs [53,55]. In ref. [53] a better practice for evaluating supercapacitor performance was suggested by evaluating the total power or energy using the cyclic voltammogram. The idea is to use the area of a cyclic voltammogram instead of some value of the current as in Eq. (13). The total power used is given by $P = \int_0^{V_c} I dV_c$. It is common to assume that all this power is associated with the capacitance C_{eff}, such that the charge accumulated is $q=C_{eff}V_c$. If this is the case, the one may write $P = \int_0^{V_c} I dV_c = \frac{dV_c}{dt} q = C_{eff} V_c \frac{dV_c}{dt}$, and the capacitance can be found according to

$$C_{eff} = \frac{\int_0^{V_c} I dV_c}{V_c \frac{dV_c}{dt}} \tag{17}$$

The blue circles in Fig. 3 b) show the computed C_{eff} from Eq. (17) for the cyclic voltammograms in Fig. 3 a). It is noted that the value of the capacitance increases monotonously from about *8 F* to about *13 F*, thus suggesting that this method gives significant systematic errors. Again, the errors occur since the resistive parts of the equivalent circuit are not considered. Thus, the method suggested in ref. [53] needs revision to function well. Assuming $t>>\tau_s$, a simple first-order correction can be made by noting that the current and voltage are related according to $I=C_1 dV_c/dt+V_c/R_1$. The area under the curve of a cyclic voltammogram is then found by integration, $\int_0^{V_c} I dV_c \approx C_1 V_c \frac{dV_c}{dt} + \frac{V_c^2}{2R_1}$, which allows us to extract the capacitance as

$$C_{eff} = C_1 \approx \frac{\int_0^{V_c} I dV_c - \frac{V_c^2}{2R_1}}{V_c \frac{dV_c}{dt}} \tag{18}$$

Simply subtracting the power dissipated in the parallel resistor is therefore a good approximation if the series resistance R_s is small and can be neglected. The blue squares in Fig. 3 b) have been computed using Eq. (18), and a value of about *10.1 F* occurs for $V_{c,max} > 1$ V, which is consistent with the value (10.3±0.2) F found using galvanostatic charging.

6. Impedance spectroscopy

Impedance spectroscopy is based on applying a small, sinusoidally varying voltage $V=V_0e^{i\omega t}$ across the supercapacitor, where $i=\sqrt{-1}$, ω is the angular frequency and t is the time. The applied voltage variations are small about a zero mean, such that the current-voltage relationship is linear for all the frequencies considered. The current through the supercapacitor is then $I=I_0e^{i\omega t}$, and the impedance is measured as $Z=V/I$.

According to the dynamic model of Fig. 1, one assumes that the supercapacitor can modelled as series of elements, where each element is a resistor R_i and a capacitor C_i in parallel. Each parallel circuit has impedance $R_i/(1+j\omega R_iC_i)$ at a given angular frequency, and the total impedance a circuit consisting of N series-connected elements is

$$Z = R_s + \sum_{i=1}^{N} \frac{R_i}{1+j\omega R_i C_i}, \tag{19}$$

where R_s is the series resistance. In the general case, one may transform this into a distribution of relaxation times $\tau_i=R_iC_i$ in order to describe the impedance of the supercapacitors, as was detailed in ref. [37]. In the current work a Randles-like circuit with $N=1$ as described in the two previous sections can be used to represent the supercapacitor studied here rather well, and the real and imaginary parts of the impedance can be written as

$$Z_{\mathrm{Re}} = R_s + \frac{R_1}{1+(\omega\tau_1)^2}, Z_{\mathrm{Im}} = -\frac{\omega\tau_1 R_1}{1+(\omega\tau_1)^2}, \tag{20}$$

where the modulus is $|Z|=\sqrt{Z_{Re}^2+Z_{Im}^2}$ and the phase is $\phi = tan^{-1}[Z_{Im}/Z_{Re}]$. The blue squares in Fig. 5 show $|Z|$ and ϕ for the supercapacitor considered in this study obtained from galvanostatic impedance spectroscopy done in the frequency range *2 mHz* to *1 MHz* with *50 mA* root-mean-square about zero average current.

The black lines in Fig. 5 a) and b) show the fit of $|Z|$ and ϕ, respectively, to the experimental data with $R_s=40\pm4$ *mΩ*, $R_1=60\pm10$ *Ω* and $C_1=11\pm1$ *F* with $R^2=0.9958$. In order to be able to describe the high-frequency experimental data, a reactive component ωL was added to Z_{Im}, where the inductance was $L=131\pm2$ *nH*. It should be noted from Fig. 5 that nearly pure capacitive behavior is displayed at frequencies below *0.5 Hz*. When making a theoretical fit to the experimental data, one could either choose to extract the capacitance entirely from the low-frequency behavior of Z_{Im}, or make a fit of the entire impedance curve which also takes into account the resistive behaviour that starts to display itself at frequencies *0.5 Hz* or above. The latter is displayed in Fig. 5 a) and gives a capacitance $C_1=11\pm1$ *F* which is in agreement with the values obtained for both galvanostatic charging and cyclic voltammetry, if uncertainties are accounted for. However, it should be pointed out that the uncertainty of the capacitance obtained using impedance spectroscopy in this manner is rather large, simply because all the data in the impedance spectrogram are equally weighted during the fit. In ref. [16] it was also pointed out that the frequencies used are of outmost important.

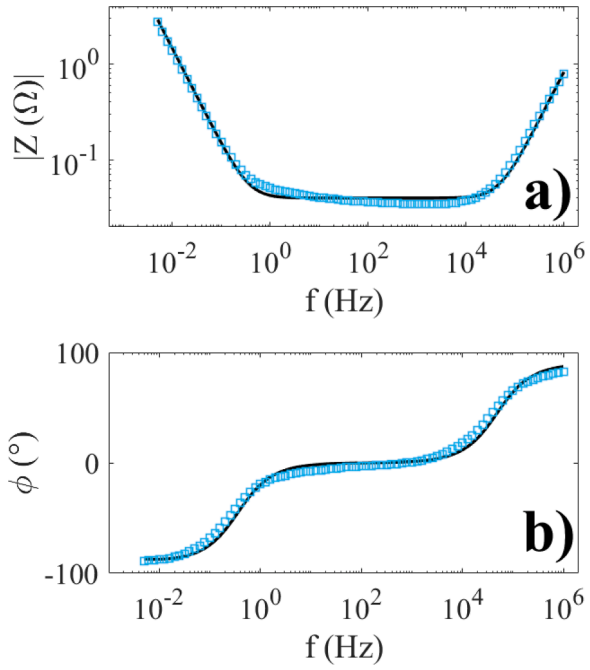

Fig. 5. Measured impedance spectrograms of the modulus (a) and phase (b) are shown as blue squares, whereas the black lines are theoretical fits to Eq. (20) with $R_s=40\pm4$ *mΩ*, $R_1=60\pm10$ *Ω*, $C_1=11\pm1$ *F* and $L=131\pm2$ *nH*(*For interpretation of the references to color in this figure legend, the reader is referred to the web version of this article.*).

From Eq. (19) it follows that for small frequencies, but as a long as $\omega\tau_i>>1$, the equivalent capacitance can be obtained as

$$\frac{1}{\sum_{i=1}^{N}\frac{1}{C_i}} = C_{eq} \approx -\frac{1}{\omega Z_{Im}}. \tag{21}$$

Eq. (21) or similar expressions is often used in the literature to determine the capacitance, and can be considered the traditional method [26]. Applied to the measured low-frequency part of the impedance spectrum between 0.01 Hz and 0.1 Hz where at the same time $\omega R_1C_1>>1$, a value of the capacitance $C_1=11.6\pm0.2$ *F* is obtained with $R^2=0.9996$. As seen above, the uncertainty of the capacitance estimate based on the whole impedance spectrum is apparently 5 times higher than that obtained using the low frequency region only, and one might be tempted to conclude that the traditional approach using Eq. (21) is therefore most suitable. However, there are two problems. First, Eq. (21) entirely neglects the real part of the measured impedance. One could argue that the real and imaginary parts of the impedance should fulfill the Kramers-Kronig relationship anyway, thus making the real part redundant. However, this is erroneous, since Eq. (21) is not exact for all frequencies. Therefore, using Eq. (21) might lead to systematic errors which cannot be revealed unless one compares the capacitance with the value obtained using galvanostatic charging and cyclic voltammetry. Indeed, the fact that the value obtained using these two latter methods both give about 10.3 F, which is about one Farad lower than the value obtained using Eq. (21), may suggest that Eq. (21) is not as accurate as one could wish. From a measurement perspective, the deviation represents a systematic error. However, it is likely that the deviation could be due to the difference in frequencies (rates) applied. It makes little sense to restrict the measurements to low frequencies where the capacitances cannot be compared with other methods in a reliable manner. A better approach is to do a fit of the theoretical formula, Eq. (19), to all the experimental data. This can be done by fitting the modulus and phase, or the real and imaginary parts, of Eq. (19) to the experimental data simultaneously. In doing so, one must expect larger uncertainties in the obtained value of the capacitance, because the model fit needs to account properly for all the parts of the impedance spectrum by assigning different resistive and capacitive elements.

It should be noted that the capacitance value obtained using the low-frequency part of the impedance data may not necessarily be consistent with the data obtained from galvanostatic charging and cyclic voltammetry, since the latter approaches apply much faster voltage variations. In Figs. 2 and 3 the voltage rate is of the order *10 mV/s* to *50 mV/s*, while for the low frequencies between *0.01 Hz* and *0.1 Hz* in Fig. 5 the voltage rate is roughly two orders of magnitude smaller. Within the equivalent circuit of Fig. 1, this can be interpreted as follows: While fast changes allow a relatively broad distribution of relaxation constants to take part in the process, only the larger time constants remain during slow charging [37], which may alter the capacitance. Thus, when comparing

the different techniques such as galvanostatic charging, cyclic voltammetry and impedance spectroscopy, one should be careful only reporting capacitance values that have been obtained using comparable applied voltage rates.

Rather slow voltage rates are investigated using impedance spectroscopy, but even slower rates occur in the case of self-discharge. The self-discharge of supercapacitors is often observed as a very slow drop in voltage after charging, and is known to be governed by slow dynamics due to for example redox-reactions, leakage currents or internal charge redistribution [56,67]. While this work has analyzed three techniques that are often used to determine capacitance, future work might also address in detail the capacitance of a supercapacitor when the slowest relaxation rates are governing the system.

7. Guidelines for extraction of capacitance of a supercapacitor

The work presented in the previous sections can be condensed into guidelines on how to extract capacitance of a supercapacitor. There are three methods; galvanostatic charging, cyclic voltammetry and impedance spectroscopy. Each technique utilizes the corresponding formulas listed in Table 1 to extract capacitance.

To this author, it appears that galvanostatic charging allows the most straightforward and easily implementable method, while both cyclic voltammetry and impedance spectroscopy require more care when extracting capacitance. The results obtained using the different techniques can only be compared if taken under similar conditions with respect to charge condition and rate of change.

Galvanostatic charging: Before galvanostatic charging is commenced, the capacitor should first be cycled a few times if it is new, and then be short-circuited without overloading it for a sufficiently long time to ensure that the voltage remains at a level comparable to the uncertainty with which measurements can be taken repeatedly (typically in the μV - mV range). One then needs to plan which current is to be used to ensure that the results are comparable to measurements obtained using cyclic voltammetry and impedance spectroscopy. To determine the capacitance using galvanostatic charging, it is recommended that one determines the initial slope of the voltage-versus-time-curve, $(dV_c/dt)_{t<<\tau i}$. Then one needs to divide the applied current I_0 with this slope to get the capacitance according to Eq. (10). Note that this procedure is different from the one usually applied. If one for example uses the average slope of the charging curve at arbitrary time intervals, one fails to include the resistive contribution. Moreover, if one decides to use any other parts of the slope at which the supercapacitor is already charged, one needs to account for the resistive contribution. A consequence of this observation is that one should be careful using the *discharge curve* for finding the capacitance. Discharge curves allow one to estimate the charge extracted, as opposed to charging curves which tells how much charge is put into a supercapacitor. Discharge curves have therefore often been assumed to be best suited for estimating the capacitance. For example, in ref. [68], the capacitance is found by dividing the applied current with slope of the *discharge curve*. However, by doing there is a danger that one might neglect the resistive contribution. If one really wishes to use the discharge curve to extract the capacitance, a suitable formula can be obtained by modifying Eq. (9) using Eq. (7) such that

$$\frac{dV_c(t)}{dt} = \sum_{i=1}^{N} \frac{I_0 - \frac{Q_i(0)}{\tau_i}}{C_i} e^{-t/\tau_i}, \tag{22}$$

where it should be remembered that $I_0<0$ and $dV_c/dt < 0$ for discharging. It is seen from Eq. (22) that the voltage-time curve becomes steeper for larger initial charges or lower time constants. That is, a discharge curve, which in general is described by Eq. (22) does not allow an easy estimate of the capacitance even for the initial part of the discharge curve $t<<\tau_i$ unless $I_0>>Q_i(0)/\tau_i$ or the time constants τ_i are already known. If these latter conditions are fulfilled, one may use Eq. (10) to extract the capacitance. However, this requires knowledge about τ_i, and the logical choice of method for extracting the capacitance is therefore galvanostatic charging starting from an uncharged state.

Cyclic voltammetry: There are no particular prerequisites preparing a supercapacitor before cyclic voltammetry, since the supercapacitor is usually cycled several times during measurement. However, one needs to make sure that Faradaic charge transfer does not appear in the cyclic voltammogram. A further discussion of this is given in the next section. The capacitance can be extracted from a cyclic voltammogram using Eq. (16), which is valid as long as the supercapacitor can be described adequately using a Randle-type equivalent circuit ($N=1$) and one wait sufficiently long time such that the current can be described by $I(t)=C_1dV_c/dt+V_c(t)/R_1$. If one instead wishes to use the area of the cyclic voltammogram to extract capacitance, it is appropriate to apply Eq. (18). For online purposes of fast capacitance evaluation, Eq. (16) might be more useful since it allows continuous monitoring of capacitance as the cyclic voltammogram is traced. On the other hand, Eq. (18) only outputs singular values of the capacitance after each complete cycle.

Impedance spectroscopy: Galvanostatic impedance spectroscopy is an impedance technique often used to study supercapacitors, and the sinusoidal current variations are usually small (e.g. in the mA range). The standard approach utilizing the imaginary part of the impedance in Eq. (21) works well as long as one is only interested in the capacitance at low frequencies, corresponding to very small voltage rates in galvanostatic charging or cyclic voltammetry. However, if one is interested in comparing the capacitance extracted at higher voltage rates with those of impedance spectroscopy, the higher frequency part of the spectrum above must also be taken into account. Under such circumstances, one should use Eq. (19) to fit the full impedance spectrum. Since the obtained capacitance is somehow a compromise of fitting the model to the full impedance spectrum, one might expect larger uncertainty in the obtained value than using Eq. (21). If Eq. (19) with N=1 does not provide an adequate fit to the experimental data, one should extract the distribution of relaxation times, as detailed in Ref. [37]. However, it should be emphasized that this is sometimes a numerically challenging task, which does not lead to singular capacitance that be used to assess supercapacitors. Under such circumstances, it might therefore be more convenient resorting to either galvanostatic charging or cyclic voltammetry.

Table 1
Essential formulas for extracting capacitance of a supercapacitor.

Method	Equation for capacitance
Galvanostatic charging	$\frac{I_0}{\left(\frac{dV_c(t)}{dt}\right)_{t\ll\tau_i}}$ Eq. (10)
Cyclic voltammetry	$\frac{I(t)-\frac{V_c(t)}{R_1}}{\frac{dV_c}{dt}}$ Eq. (16), $\frac{\int_0^{V_c} IdV_c - \frac{V_c^2}{2R_1}}{V_c\frac{dV_c}{dt}}$ Eq. (18)
Impedance spectroscopy	Fit Eq. (19) to experimental data, $R_s + \sum_{i=1}^{N}\frac{R_i}{1+j\omega R_i C_i}$ Eq. (19)

8. Extension to pseudocapacitors

The guidelines presented in the previous section were made under the assumption that charge storage is governed by the electrical double layer. This is the case in many carbon-based supercapacitors. Under some circumstances redox-reactions might be present in carbon-based supercapacitors, due to for example the presence of minor amounts of oxygen [61], but these are most often parasitic and therefore do not contribute to charge storage. Such parasitic redox-reactions can be modelled using resistors in the equivalent circuit of Fig. 1 as long as the response is linear. Under circumstances where linearity fails, one needs to subtract the nonlinear contribution.

Pseudocapacitors are supercapacitors based on for example

conducting polymers, nitrides or transition-metal oxides, where the charge can be stored either in a non-Faradaic manner in the electrical double layer as well as through Faradaic electron transfer associated with redox-reactions. It should also be pointed out that by for example treating carbon nanostructures with acids has been suggested as a method to increase the charge storage possibly in a Faradaic manner [69], although it has not entirely been ruled out that an increased contribution of the electrical double layer could contribute as well. In general, it is challenging to use a single measurement technique based on current-voltage measurements to differentiate between parasitic redox-reactions that do not contribute to charge storage, and redox-reaction that do contribute to charge storage. One therefore needs common ways to describe charge storage in a pseudocapacitor. To this end, a good question is whether capacitance is a suitable way to represent the charge storage capability, or if it instead should be measured directly as the charge that can be extracted from a loaded pseudocapacitor.

It has been stated that both non-Faradaic charge storage in the electrical double layer as well as Faradaic charge transfer associated with redox-reactions give rise to a current that is proportional to the charge rate [45,46]. The model in Section 2 demonstrated how this works for the electrical double layer. A simple near-equilibrium model valid for redox-reactions based on localized electrons and low scanning rates can be used to illustrate the contribution of Faradaic charge transfer to the current during cyclic voltammetry [70,71]. Consider a redox-reaction where ox+ne$^-$↔red, where ox is the oxidized species, red is the reduced species, and n is the moles of electrons e$^-$. If the standard redox-potential is E^0 and the mole-fractions of oxidized and reduced species are X_{ox} and X_{red}, respectively, the potential of the redox-reaction can be approximated by the Nernst equation

$$E = E^0 + \frac{RT}{nF} ln\left(\frac{X_{ox}}{X_{red}}\right), \tag{22}$$

and the current can be found as [70,71]

$$I_{redox} = a\frac{dV_c}{dt}\frac{e^{\frac{nF}{RT}\left(E-E^0\right)}}{\left[1+e^{\frac{nF}{RT}\left(E-E^0\right)}\right]^2}, \tag{23}$$

where a is a constant, R is the universal gas constant and T is the temperature. It is seen that the current due to this redox-reaction is proportional to the scan rate dV_c/dt during cyclic voltammetry, which is the same behavior one expects from a electrical double layer supercapacitor. However, the nonlinear peak-shaped behavior associated with a single peak such as that exhibited by Eq. (23) does not allow extraction of a reliable capacitance value.

As pointed out in ref. [71], the galvanostatic charge-discharge curve can be obtained by linking the mole fraction of the reduced or oxidated species to the current passed in Eq. (22). This gives rise to voltage versus time curves which first quickly grow with time, then remain almost constant for a while, before quickly growing again. This is very far from the behavior normally associated with a capacitor, and a capacitance cannot be reliably determined if the redox-reaction is due to localized electrons governed by Nernstian dynamics as described by Eq. (22). For such situations where localized electrons govern the behavior it is probably more convenient and accurate to directly let the charge extracted out of the device to be a measure of its ability to store charge.

In some cases, the redox-reactions might be governed by delocalized electrons [70], which allow a large number of peaks which eventually sum up to a very broad peak which gives rise to cyclic voltammograms and charging curves that resemble those of electrical double layer supercapacitors. The cyclic voltammogram as well as the galvanostatic charging curve will now look almost like that of a supercapacitor based on an electrical double layer charge storage. Examples of such curves are shown in Fig. 6.

Let us first try to analyze the case of cyclic voltammetry as depicted in Fig. 6 a). In analogy with Eqs. (1) and (16), the current is given $I=C_{pseudo}dV_c/dt+V_c(t)/R_1+I_{redox}+I_p$, where I_{redox} is the Faradaic charge transfer rate associated with localized electrons which in some cases can be described using Eq. (23), while I_p is due to parasitic redox-reactions near the end of the potential window. The two latter are nonlinear contributions that must be added to the linearized Eq. (1) to get a reasonable model of the system. By doing so, one assumes that the currents are additive, which is a simplifying model assumption that must be checked independently by experiments. The parasitic current represented by I_p is often described phenomenologically by the Butler-Volmer equation [70].

The solid, black line in Fig. 6 a) shows a typical cyclic voltammogram for a pseudocapacitor, containing both singular peaks due to redox-reactions of localized electrons as well as a broad distribution of peaks due to delocalized electrons. Upon subtracting the singular redox-peak and the parasitic contribution, i.e. finding I- $(I_{redox}+I_p)$, the dotted red curve in Fig. 6 a) remains. One now has I- $(I_{redox}+I_p)=C_{pseudo}dV_c/dt+V_c(t)/R_1$, where the capacitance C_{pseudo} can be found in the same manner as described in the previous section electrical double layer supercapacitors. The blue, dashed curve in Fig. 6 a) illustrates the final curve resembling that of an electrical double-layer supercapacitor without resistive contributions. However, one should note that both Faradaic and non-Faradaic charge storage mechanisms might both be governing the behavior, despite its apparent similarity with that of an ideal capacitor. Thus, if one is going to use the procedure for cyclic voltammetry described in the previous section on pseudocapacitors, one first has to remove the contributions that are due to both isolated redox centers as well as parasitic contributions. A problem with this approach is that it is hard to extract both I_{redox} and I_p independently and in a reliable manner, thus leaving the remaining determination of C_{pseudo} prone to systematic errors. In ref. [71] both I_{redox} and I_p, in addition to the ohmic contributions were associated with a 'contribution' to the capacitance as obtained from a single cyclic voltammogram. Here, I argue that comparing contributions to capacitance in this manner would be misleading, since technically one can only speak about capacitance in a manner that allows comparison between techniques if the cyclic voltammogram has the shape that allows proper comparison. If this is not case, one should instead identify the charge storage mechanisms separately, and rather report the charge stored instead of the capacitance.

Based on the observations made for cyclic voltammetry, it is now possible to discuss the case of the galvanostatic charging as depicted in Fig. 6 b). Eq. (10) can be used also in this case if it is known that the contribution is due to the delocalized electrons causing Faradaic charge

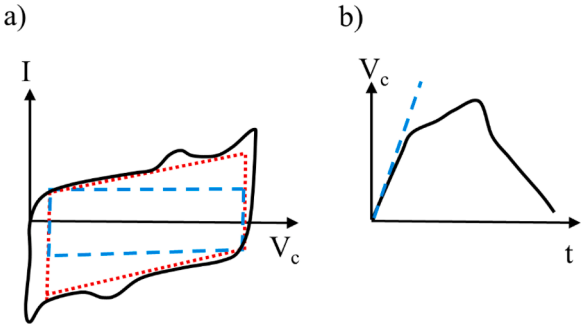

Fig. 6. In a) the full cyclic voltammogram is shown as a solid, black line. The dotted, red line is obtained by subtracting the current due to redox peaks associated with localized electrons as well as parasitic redox reactions. The blue, dashed line is obtained after subtracting the resistive contribution from the red, dotted line. In b), the solid black line is the full galvanostatic charge-discharge curve, whereas the blue dashed line is a linear fit to the initial charging curve(For interpretation of the references to color in this figure legend, the reader is referred to the web version of this article.).

transfer as discussed above. To this end, it is often possible to select a potential window wherein the contribution from redox peaks or other parasitic contributions are negligible. The method utilizing galvanostatic charging and Eq. (10) works at low potentials, which means that this procedure should in many cases be directly applicable also to pseudocapacitors as well. However, again it is important to stress that the obtained value of capacitance from Eq. (10) does not take into account singular redox-peaks, which should be reported separately as charge stored.

Finally, it could be mentioned that the assumptions of small polarization discussed above should also allow Eq. (19) to be applicable for extraction of capacitance using impedance spectroscopy. However, pseudocapacitors will most likely require $N>1$ and therefore be represented by more than a single capacitance value. However, a further discussion of this is outside the scope of the current work.

8. Conclusion

The aim of this work has been to propose methods for consistently extracting capacitance values associated with an equivalent circuit using galvanostatic charging, cyclic voltammetry and impedance spectroscopy. Several different methods are considered, and their benefits and shortcomings are discussed. While the current work is concerned with carbon-based supercapacitors utilizing charge storage associated with the electrical double layer, it is discussed how the methods can be extended to pseudocapacitors as well, thus providing a tool for consistently reporting capacitance of such devices.

Declaration of Competing Interest

The authors declare that they have no known competing financial interests or personal relationships that could have appeared to influence the work reported in this paper.

References

[1] H.I. Becker, U.S. pat., 2800.616 to General Electric Co, 1957.
[2] B.E. Conway, Electrochemical Supercapacitors, Kluwer Academic, New York, USA, 1999.
[3] J.R. Miller, Engineering electrochemical capacitor applications, J. Power Sources 326 (2016) 726–735.
[4] L.M. Da Silva, R. Cesar, C.M.R. Moreira, J.H.M. Santos, L.G. De Souza, B.M. Pires, R. Vincentini, W. Nunes, H. Zanin, Reviewing the fundamentals of supercapacitors and the difficulties involving the analysis of the electrochemical findings obtained for porous electrode materials, Energy Storage Mater. 27 (2020) 555–590.
[5] D.P. Dubal, Y.P. Wu, R. Holze, Supercapacitors: from the Leyden jar to electric buses, ChemTexts 2 (2016) 13.
[6] Q. Dou, H.S. Park, Perspective on high-energy carbon-based supercapacitors, Energy Environ. Mater. 3 (2020) 286–305.
[7] H. Shao, Y.C. Wu, Z. Li, P.L. Taberna, P. Simon, Nanoporous carbon for electrochemical capacitive energy storage, Chem. Soc. Rev. 49 (2020) 3005.
[8] J. Xie, P. Yang, Y. Wang, T. Qi, Y. Lei, C.M. Li, Puzzles and confusions in supercapacitor and battery: theory and solutions, J. Power Sources 401 (2018) 213–223.
[9] C. Pean, B. Rotenberg, P. Simon, M. Salanne, Multi-scale modelling of supercapacitors: from molecular simulations to a transmission line model, J. Power Sources 326 (2016) 680–685.
[10] M. Kroupa, G.J. Offer, J. Kosek, Modelling of supercapacitors: factors influencing performance, J. Electrochem. Soc. 163 (2016). A2475-A2487.
[11] R.L. Spyker, R.M. Nelms, Classical equivalent circuit parameters for a double-layer capacitor, IEEE Trans. Aerosp. Electron. Syst. 36 (2000) 829–836.
[12] L. Zubieta, R. Bonert, Characterization of double-layer capacitors for power electronics applications, IEEE Trans. Ind. Appl. 36 (2000) 199–205.
[13] H. Gualous, D. Bouquain, A. Berthon, J.M. Kauffmann, Experimental study of supercapacitor serial resistance and capacitance variations with temperature, J. Power Sources 123 (2003) 86–93.
[14] F. Rafika, H. Gualous, R. Gallay, A. Crausaz, A. Berthon, Frequency, thermal and voltage supercapacitor characterization and modeling, J. Power Sources 165 (2007) 928–934.
[15] R. Faranda, A new parameters identification procedure for simplified double layer capacitor two-branch model, Electr. Pow. Syst. Res. 80 (2010) 363–371.
[16] C. Lämmel, M. Schneider, M. Weiser, A. Michaelis, Investigations of electrochemical double layer capacitor (EDLC) materials - a comparison of test methods", Mat.-wiss, U. Werkstofftech. 44 (2013) 641–649.
[17] R. Chai, Y. Zhang, A practical supercapacitor model for power management in wireless sensor nodes, IEEE Trans. Pow. Electron. 30 (2015) 6720–6730.
[18] P. Saha, S. Dey, M. Khanra, Accurate estimation of state-of-charge of supercapacitor under uncertain leakage and open circuit voltage map, J. Power Sources 434 (2019), 226696.
[19] A. Weddell, G. Merrett, T. Kazmierski, B. Al-Hashimi, Accurate supercapacitor modeling for energy harvesting wireless sensor nodes, IEEE Trans. Circuits Syst, II Exp Briefs 58 (2011) 911–915.
[20] Y. Zhang, H. Yang, Modeling and characterization of supercapacitors for wireless sensor network applications, J. Power Sources 196 (2011) 4128–4135.
[21] H. Yang, Y. Zhang, A study of supercapacitor charge redistribution for applications in environmentally powered wireless sensor nodes, J. Power Sources 273 (2015) 223–236.
[22] H. Yang, Y. Zhang, Characterization of supercapacitor models for analyzing supercapacitors connected to constant power elements, J. Power Sources 312 (2016) 165–171.
[23] S. Rajput, A. Kuperman, A. Yahalom, M. Averbukh, Studies on dynamic properties of ultracapacitors using infinite r-C chain equivalent circuit and reverse Fourier transform, Energies 13 (2020) 4583.
[24] S. Buller, E. Karden, D. Kok, R. Doncker, Modeling the dynamic behavior of supercapacitors using impedance spectroscopy, IEEE Trans. Ind. Appl. 38 (2002) 1622–1626.
[25] Y. Parvini Y, J.B. Siegel, A.G. Stefanopoulou, A. Vahidi, Supercapacitor electrical and thermal modeling, identification, and validation for a wide range of temperature and power applications, IEEE Trans. Ind. Electron. 63 (2016) 1574–1585.
[26] N. Devillers, S. Jemei, M.C. Péra, D. Bienaimé, F. Gustin, Review of characterization methods for supercapacitor modelling, J. Power Sources 246 (2014) 596–608.
[27] L. Zhang L, Z. Wang Z, X. Hu, F. Sun, D.G. Dorrell, A comparative study of equivalent circuit models of ultracapacitors for electric vehicles, J. Power Sources 274 (2015) 899–906.
[28] I.N. Jiya, N. Gurusinghe, R. Gouws, Electrical circuit modelling of double layer capacitors for power electronics and energy storage applications: a review, Electronics 7 (2018) 268.
[29] Q.A. Huang, Y. Li, K.C. Tsay, C. Sun, C. Yang, L. Zhang, J. Zhang, Multi-scale impedance model for supercapacitor porous electrodes: theoretical prediction and experimental validation, J. Power Sources 400 (2018) 69–86.
[30] S. Satpathy, S. Das, B.K. Bhattacharyya, How and when to use super-capacitors effectively, an integration of review of past and new characterization works on super-capacitors, J. Energy Storage 27 (2020), 101044.
[31] Y. Abetbool, S. Rajput, A. Yahalom, M. Averbukh, Comprehensive study on dynamic parameters of symmetric and asymmetric ultracapacitors, Electronics 8 (2019) 891.
[32] A. Berrueta, A. Ursua, I.S. Marin, A. Eftekhari, P. Sanchis, Supercapacitors: electrical characteristics, modeling, applications and future trends, IEEE Access 7 (2019) 50869–50896.
[33] R. Vicentini, L.M. Da Silva, E.P.C. Junior, T.A. Alves, W.G. Nunes, H. Zanin, How to measure and calculate equivalent series resistance of electrical double layer capacitors, Molecules 24 (2019) 1452.
[34] Y. Zhao, W. Xie, Z. Fang, S. Liu, A parameters identification method of the equivalent circuit model of the supercapacitor cell module based on segmentation optimization, IEEE Access 8 (2020) 92895–92906.
[35] D. Xu, L. Zhang, B. Wang, G. Ma, Modeling of supercapacitor behavior with an improved two-branch equivalent circuit, IEEE Access 7 (2019) 26379–26390.
[36] C. Liu, Y. Wang, Z. Chen, Q. Ling, A variable capacitance based modeling and power capability predicting method for ultracapacitor, J. Power Sources 374 (2018) 121–133.
[37] L.E. Helseth, Modelling supercapacitors using a dynamic equivalent circuit with a distribution of relaxation times, J. Energy Storage 25 (2019), 100912.
[38] B. Wang, C. Wang, Q. Hu, L. Zhang, Z. Wang, Modelling the dynamic self-discharge effects of supercapacitors using a controlled current source based ladder equivalent circuit, J. Energy Storage 30 (2020), 101473.
[39] G. Navarro, J. Najera, J. Torres, M. Blanco, M. Santos, M. Lafoz, Development and experimental validation of a supercapacitor frequency domain model for industrial energy applications considering dynamic behavior at high frequencies, Energies 13 (2020) 1156.
[40] R.J. Hunter, Introduction to Modern Colloid Science, 1st ed., Oxford Science Publications, 1993.
[41] H. Wang, L. Pilon, Intrinsic limitations of impedance measurements in determining electric double layer capacitances, Electrochim. Acta 63 (2012) 55.
[42] B. Roling, M. Drűschler, Comments on "Intrinsic limitations of impedance measurements in determining electric double layer capacitances", Electrochim. Acta 76 (2012) 526–528.
[43] H. Wang, L. Pilon, Reply to comments on "Intrinsic limitations of impedance measurements in determining electric double layer capacitances, Electrochim. Acta 76 (2012) 529–531.
[44] D.K. Kampouris, X. Ji, E.P. Randviir, C.E. Banks, A new approach for the improved interpretation of capacitance measurements for materials utilized in energy storage, RSC Advances 5 (2015) 12782–12791.
[45] Y. Ge, X. Xie, J. Roscher, R. Holze, Q. Qu, How to measure and report the capacity of electrochemical double layers, supercapacitors, and their electrode materials, J. Solid State Electrochem. 24 (2020) 3215–3230.
[46] Y. Gogotsi, R.M. Penner, Energy storage in nanomaterials – capacitive, pseudocapacitive, or battery-like, ACS Nano 12 (2018) 2081–2083.

[47] Y. Jiang, J. Liu, Definitions of pseudocapacitive materials: a brief review, Energy Environ. Mater. 2 (2019) 30–37.
[48] H. Yang, A comparative study of supercapacitor capacitance characterization methods, J. Energy Storage 29 (2020), 101316.
[49] G.G.G. Costa, R. Pietronero, T. Catunda, The internal resistance of supercapacitors, Phys. Educ. 47 (2012) 439–443.
[50] X. Du, C. Wang, M. Chen, Y. Jiao, J. Wang, Electrochemical performance of nanoparticle Fe_3O_4/activated carbon supercapacitor using KOH electrolyte, J. Phys. Chem. 113 (2009) 2643–2646.
[51] MP. Down, C.W. Foster, X. Ji, C.E. Banks, Pencil drawn paper based supercapacitors, RSC Adv. 6 (2016) 81130–81141.
[52] X. Zhang, X. Wang, L. Jiang, H. Wu, C. Wu, J. Su, Effect of aqueous electrolytes on the electrochemical behaviors of supercapacitors based on hierarchically porous carbon, J. Power Sources 216 (2012) 290–296.
[53] P. Yang, W. Mai, Flexible solid-state electrochemical supercapacitors, Nano Energy 8 (2014) 274–290.
[54] X. Wang, R.S. Chandrabose, S.E. Chun, T. Zhang, B. Evanko, Z. Jian, S. W. Boettcher, G.D. Stucky, X. Ji, High energy density aqueous electrochemical capacitors with a KI-KOH electrolyte, ACS Appl. Mat. Int. 7 (2015) 19978–19985.
[55] Y. Huang, M. Zhong, Y. Huang, M. Zhu, Z. Pei, Z. Wang, Q. Xue, X. Xie, C. Zhi, A self-healable and highly stretchable supercapacitor based on a dual crosslinked polyelectrolyte, Nat. Commun. 6 (2015) 10310.
[56] B.E. Conway, W.G. Pell, T.C. Liu, Diagnostic analyses for mechanisms of self-discharge of electrochemical capacitors and batteries, J. Power Sources 65 (1997) 53–59.
[57] B.W. Ricketts, C. Thon-That, Self-discharge of carbon-based supercapacitors with organic electrolytes, J. Power Sources 89 (2000) 64–69.
[58] M. Kaus, J. Kowal, D.U. Sauer, Modelling the effects of charge redistribution during self-discharge of supercapacitors, Electrochim. Acta 55 (2010) 7516–7523.
[59] J. Kowal, E. Avaroglu, F. Chamekh, A. Seinfelds, T. Thien, D. Wijaya, D.U. Sauer, Detailed analysis of the self-discharge of supercapacitors, J. Power Sources 196 (2011) 573–579.
[60] P. Kurzweil, M. Shamonin, State-of-charge monitoring by impedance spectroscopy during long-term self-discharge of supercapacitors and lithium-ion batteries, Batteries 4 (2018) 35.
[61] H.A. Andreas, Self-discharge in electrochemical capacitors: a perspective article, J. Electrochem. Soc. 162 (2015) A5047–A5053.
[62] J. Black, H.A. Andreas, Effects of charge redistribution on self-discharge of electrochemical capacitors, Electrochim. Acta 54 (2009) 3568–3574.
[63] J. Black, H.A. Andreas, Predictions of the self-discharge profile of an electrochemical capacitor electrode in the presence of both activation-controlled discharge and charge redistribution, J. Power Sources 195 (2010) 929–935.
[64] A.M. Oickle, J. Tom, H.A. Andreas, Chemical oxidation and its influence on self-discharge in aqueous electrochemical capacitors, Carbon 110 (2016) 232–242.
[65] A. Lewandowski, P. Jakobczyk, M. Galinski, M. Biegun, Self-discharge of electrochemical double layer capacitors, Phys. Chem. Chem. Phys. 15 (2013) 8692.
[66] J.W. Graydon, M. Panjehshahi, D.W. Kirk, Charge redistribution and ionic mobility in the micropores of supercapacitors, J. Power Sources 245 (2014) 822–829.
[67] V. Sedlakova, J. Sikula, J. Mazner, P. Sedlak, T. Kuparowitz, B. Buergler, P. Vasina, Supercapacitor equivalent circuit model based on charges redistribution by diffusion, J. Power Sources 286 (2015) 58–65.
[68] R. Heimböckel, F. Hoffmann, M. Fröba, Insights into the influence of the pore size and surface area of activated carbons on the energy storage of electric double layer capacitors with a new potentially universally applicable capacitor model, Phys. Chem. Chem. Phys. 21 (2019) 3122.
[69] L. Guan, L. Yu, G.Z. Chen, Capacitive and non-capacitive faradaic charge storage, Electrochim. Acta 206 (2016) 464–478.
[70] G.Z. Chen, Supercapacitor and supercapattery as emerging electrochemical energy stores, Int. Mat. Rev. 62 (2017) 173–202.
[71] H.M. Fellows, M. Forghani, O. Crosnier, S.W. Donne, Modelling voltametric data from electrochemical capacitors, J. Power Sources 417 (2019) 193–206.